IOPscience iopscience.iop.org

Home Search Collections Journals About Contact us My IOPscience

Electrical conduction mechanisms in thermally evaporated tungsten trioxide (WO_3) thin films

This article has been downloaded from IOPscience. Please scroll down to see the full text article.

2006 J. Phys.: Condens. Matter 18 9987

(http://iopscience.iop.org/0953-8984/18/44/001)

View the table of contents for this issue, or go to the journal homepage for more

Download details:
IP Address: 129.252.86.83
The article was downloaded on 28/05/2010 at 14:27

Please note that terms and conditions apply.

Institute of Physics Publishing — Journal of Physics: Condensed Matter

J. Phys.: Condens. Matter **18** (2006) 9987–9997 doi:10.1088/0953-8984/18/44/001

Electrical conduction mechanisms in thermally evaporated tungsten trioxide (WO_3) thin films

M G Hutchins[1], **O Abu-Alkhair**[2], **M M El-Nahass**[3,5] **and K Abdel-Hady**[4]

[1] School of Engineering, Oxford Brookes University, Oxford, UK
[2] Physics Department, Faculty of Science, King Abdel-Aziz University, Jeddah, Saudi Arabia
[3] Physics Department, Faculty of Education, Ain Shams University, Cairo 11757, Egypt
[4] Physics Department, Faculty of Science, Minia University, Menia, Egypt

E-mail: prof_nahhas@yahoo.com

Received 21 May 2006, in final form 7 August 2006
Published 20 October 2006
Online at stacks.iop.org/JPhysCM/18/9987

Abstract
Thin films of amorphous tungsten trioxide, a-WO_3, have been thermally evaporated onto glass substrate held at 350 K. Annealing at 723 K caused the formation of polycrystalline tungsten trioxide, c-WO_3, with a monoclinic structure. The dark DC electrical conductivity of both a-WO_3 and c-WO_3 was studied over a temperature range from 298 to 625 K in two environmental conditions (air and vacuum). A simple Arrhenius law, a polaron model and a variable range hopping model have been used to explain the conduction mechanism for a-WO_3 films. Using the variable range hopping model, the density of localized states at the Fermi level, $N(E_F)$, was found to be 1.08×10^{19} eV^{-1} cm^{-3}. The mechanism of electrical conduction in c-WO_3 films is explained by means of the Seto model. The Seto model parameters were determined as the energy barrier ($E_b = 0.15$ eV), the energy of trapping states with respect to the Fermi level ($E_t = 0.9$ eV) and the impurity concentration ($N_D = 4.05 \times 10^{15}$ eV^{-1} cm^{-3}). The thickness dependence of resistivity of c-WO_3 films has been found to decrease markedly with increasing film thickness, which is explained on the basis of the effective mean free path model. Using this model, the mean free path of electrons in c-WO_3 films was evaluated. The temperature dependence of the thermoelectric power for a-WO_3 films reveals that our samples are n-type semiconductors.

1. Introduction

Semiconducting oxide glasses are technologically important as insulating materials as well as optical glasses. However, heavy metal oxide glasses containing lead or tungsten have a reputation of being good materials for IR transmission, and have electrochromic, photochromic and ferroelectric like behaviour [1–3].

[5] Author to whom any correspondence should be addressed.

 © 2006 IOP Publishing Ltd Printed in the UK

Tungsten trioxide thin films have been extensively studied because of their potential application in electrochromic devices. The optical properties of these films can be changed in a reversible and persistent way under the influence of an applied voltage. It is widely accepted that the electrochromic process involves the simultaneous injection (or extraction) of electrons and charge compensating ions into interstitial sites of the WO_3 matrix [4]. For polycrystalline films, the injected electrons behave as free-carriers, leading to an increase in the near infrared reflectivity [5]. Tungsten oxide is a transition metal oxide (TMO) which has two different valence states, namely W^{5+} and W^{6+}. The hopping of electrons between these two valence states appears to be responsible for the conduction in this type of glass [6]. Therefore the nature of the TMO ions and the concentration of ions in the reduced states determine the conductivity behaviour. The concentration ratio of both valence states can be altered by the nature of the host glass, its composition and the preparation conditions.

The physical properties of a material are greatly affected by the structural order and surface morphology. Different preparative methods have respective advantages in film quality and production cost from the viewpoint of material applications. More recently, amorphous tungsten oxide (a-WO_3) and crystalline tungsten oxide (c-WO_3) thin films prepared by various methods, including sputtering [7–10], pulsed laser [11, 12], thermal evaporation [13–15], wet chemical method [16–21], sol–gel [22], and spray pyrolysis [23, 24], have been investigated.

In fact, a-WO_3 films show pronounced transmission modulation in both the visible and solar spectral range when intercalated with protons (H^+) or lithium ions (Li^+), based on absorption modulation. This leads to the adverse effect of a high-temperature condition within the device. In contrast, c-WO_3 becomes reflective in the near infrared when charge is inserted [10, 25], offering the possibility to develop variable transmission devices in which reflectance modulation is the dominant behaviour. Moreover, c-WO_3 films play a fundamental role in gas sensing properties [24].

Development of devices based on WO_3 thin films is clearly dependent upon knowledge of the general electrical behaviour of these materials. Therefore, the aim of the present work is to study the conduction mechanisms in thermally evaporated WO_3 thin films by fitting the experimental results with various theoretical models.

2. Experimental details

The WO_3 powder used in this study was obtained from BDH Chemical Company Ltd, with purity of 99.986%. Thin films of different thicknesses were deposited by vacuum thermal evaporation, using a high-vacuum coating unit (Edwards, E306A). The films were deposited onto pre-cleaned glass substrates maintained at 350 K. Thin films were deposited from a molybdenum evaporator charged by WO_3 in a vacuum of 10^{-4} Pa. The film thickness and the deposition rate (1 nm s^{-1}) were controlled by using a quartz crystal thickness monitor (Edwards, FTM6) and the film thickness was pre-calibrated interferometrically. Then the films were annealed at 723 K for 2 h in air. In our previous work [15], we observed that the as-deposited films are amorphous in nature and exhibit a broad peak around $2\theta = 23°$ in the x-ray diffraction pattern. Transformation from amorphous to crystalline occurred at the annealing condition of 723 K for 2 h in air.

The dark DC electrical resistivity of WO_3 thin films was measured under vacuum of 10^{-2} Pa by the two-probe method in the temperature range from 298 to 625 K using a high internal impedance electrometer (Keithley 617A), while the temperature was measured using a chromel–alumel thermocouple. Ohmic contacts were achieved by evaporating gold electrodes. For the thermoelectric power measurements, copper electrodes were deposited onto the two ends of the samples. The Seebeck coefficient was measured within the temperature range 290–370 K.

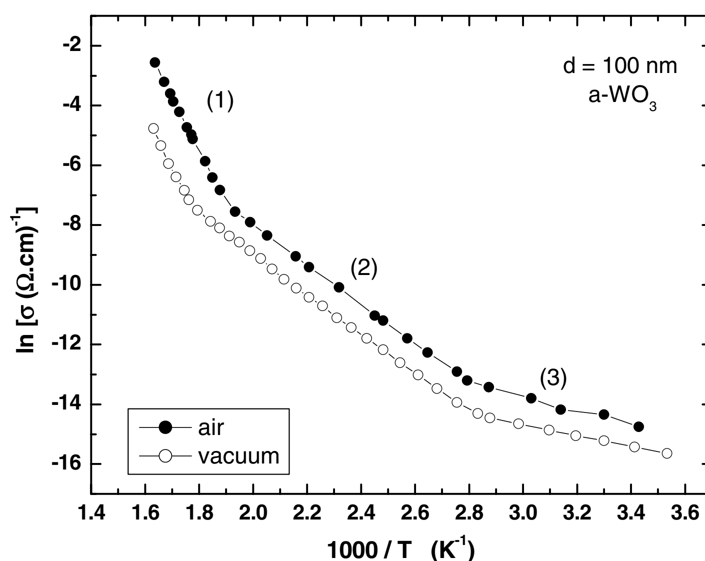

Figure 1. The relation between $\ln \sigma$ and $1000/T$ for a-WO_3 films in air and vacuum conditions.

3. Results and discussion

3.1. DC conductivity measurements

3.1.1. Amorphous WO_3 films. The dark electrical conductivity, σ, as a function of temperature for a-WO_3 film with thickness 100 nm, as a representative sample, in two environmental conditions (air and vacuum) is depicted in figure 1. It shows that σ increases exponentially with temperature. The conductivity is higher, by one order, in films measured in air than of those measured in vacuum. This behaviour is normal for semiconductor metal oxide gas sensors due to their high sensitivity to the presence of various gases in the ambient atmosphere, which can be attributed to the increase of carrier concentration in films measured in air resulting from both adsorbed and absorbed gases atoms, which act as acceptor impurities [26].

In inorganic semiconductors, the semiconducting properties are brought about by thermal excitation, impurities and lattice defects. Holes in the valence band and electrons in the conduction band contribute to the electrical conductivity. If we assume that the variation of mobility of the electrons and holes in an electric field with temperature is small, then the conductivity is proportional to the number of carriers.

Conductivity in transition metal oxides is due to both hopping of electrons and charge transport via excited states. In such a case, the conductivity is given by [27]

$$\sigma = A_1 \exp(-\Delta E_1/k_B T) + A_2 \exp(-\Delta E_2/k_B T) + A_3 \exp(-\Delta E_3/k_B T) + \cdots, \qquad (1)$$

where ΔE_1 is the activation energy for intrinsic conduction and ΔE_2, $\Delta E_3, \ldots$ are the activation energies needed for hopping conduction. A_1, A_2, A_3 are constants and k_B is the Boltzmann constant.

Figure 1 shows $\ln \sigma$ versus $1000/T$ as obtained experimentally. These results indicate that the conduction is through an activated process having three conduction levels. The obtained slopes of these different regions were found to be independent of film thickness, which indicated that the activation energies are independent of the film thickness in the thickness range 100–185 nm. The average values of activation energies were found to be 1.70, 0.58 and 0.06 for ΔE_1, ΔE_2 and ΔE_3, respectively.

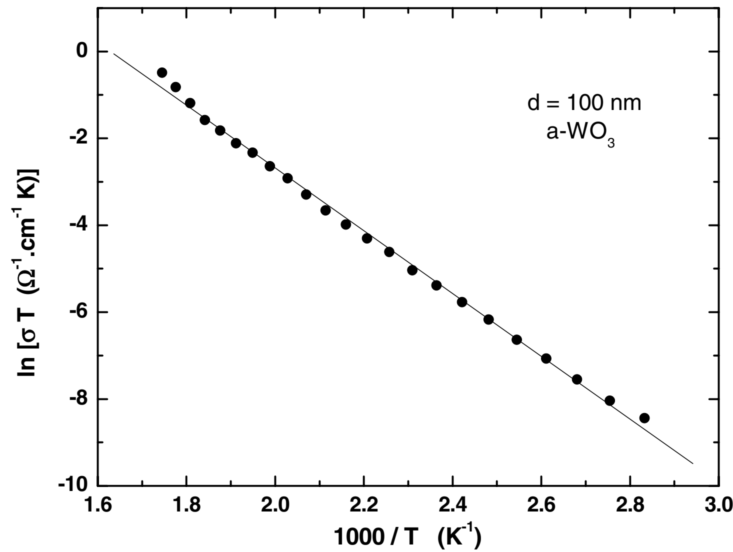

Figure 2. The relation between $\ln \sigma T$ and $1000/T$ for a-WO_3 films in vacuum condition.

In order to obtain a clear distinction between these three conduction mechanisms, three models are used to fit the high-temperature conductivity data on transition metal oxide, namely, a simple Arrhenius law [28], a polaron model and a variable-range hopping (VRH) model [29, 30].

For the first regime $T > 520$ K, the conductivity mechanism is due to intrinsic conduction. The conductivity can be expressed by the relation [28]

$$\sigma = \sigma_0 \exp(-\Delta E_1/k_B T), \tag{2}$$

where σ_0 is a pre-exponential factor and ΔE_1 is the activation energy, which is found to vary between 1.69 and 1.72 eV with a mean value of 1.70 eV, being approximately half the band gap of WO_3; this is in agreement with the estimated band gap from the absorption spectrum of a-WO_3 [15].

The interaction between the electrons and the lattice is strong enough to form small polarons [31, 32]. This is why transport of electrons in transition metal oxide glasses is usually termed as 'small-polaron hopping'. In the second temperature regime, $525 \text{ K} \leqslant T \leqslant 353$ K, the conductivity of a-WO_3 thin films can be interpreted in terms of the phonon-assisted hopping model given by Mott [29, 30]:

$$\sigma = \frac{e^2 \nu_{ph} c(1-c)}{k_B T R} \exp(-2\alpha R) \exp(-W/kT), \tag{3}$$

where ν_{ph} is the optical phonon frequency, R is the average spacing between the transition ions, and α is the localization length. In addition, c is the fraction of reduced transition metal ions (the ratio of ion concentration of transition metal ions in the low valence state to the total concentration of transition metal ions) and W is the activation energy for the hopping conduction. Equation (3) describes a non-adiabatic regime of small-polaron hopping and is usually used to analyse the σ_{DC} of glasses containing transition metal oxides such as iron oxide. Figure 2 illustrates the relation between $\ln \sigma T$ and $1000/T$ for a-WO_3 thin films. Assuming that ν_{ph} and R are constant, the activation energy, W, is calculated from the slope of the straight line and is found to be 0.62 eV.

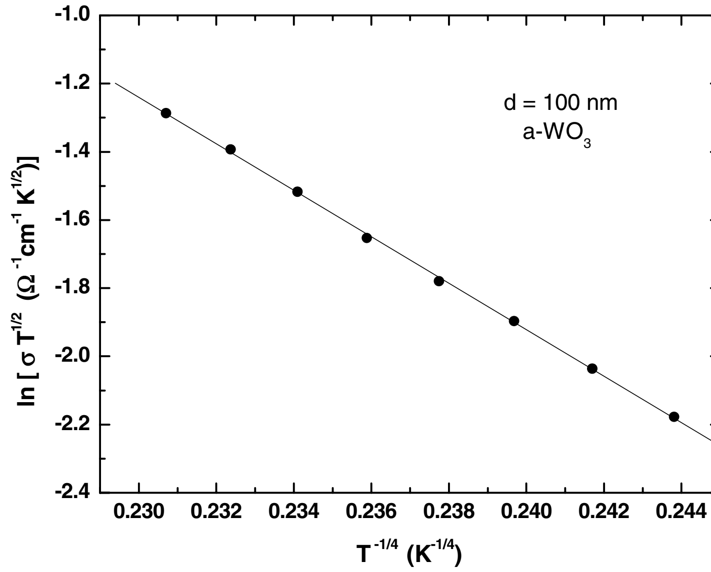

Figure 3. The relation between $\ln(\sigma T^{1/2})$ and $T^{-1/4}$ for a-WO_3 films in vacuum condition.

According to conventional small-polaron theory, the activation energy should decrease to zero (band conduction) at low temperature; the VRH model of small polarons also predicts continuously decreasing activation energy with decreasing temperature [33]. The procedure suggested by Greaves [33] as a modification of Mott's model of VRH [28] could be applied in the third temperature regime ($T \leqslant 353$ K), and the following expression is proposed for the DC conductivity:

$$\sigma T^{1/2} = A \exp(-BT^{-1/4}), \tag{4}$$

where A and B are constants; B is given by

$$B = 2.1[\alpha^3/k_B N(E_F)]^{1/4}. \tag{5}$$

$N(E_F)$ is the density of localized states at E_F and α^{-1} is the decay constant of the wavefunction of localized states at E_F. A plot of $\ln(\sigma T^{1/2})$ versus $T^{-1/4}$ is shown in figure 3. A good fit of the experimental data to expression (4) in this temperature range suggests that Greaves variable range hopping may be valid in this region. The values of parameters A and B were calculated from this curve; they are $1.86 \times 10^6\ \Omega^{-1}\ \text{cm}^{-1}\ \text{K}^{1/2}$ and $68.17\ \text{K}^{1/4}$ respectively. In addition, the density of localized states at the Fermi level, $N(E_F)$, has been calculated taking a constant value of α^{-1} (10^{-7} cm), and it was found to be $1.08 \times 10^{19}\ \text{eV}^{-1}\ \text{cm}^{-3}$.

3.1.2. Crystalline WO_3 films. To study the effect of c-WO_3 film thickness on its electrical resistivity, films of different thicknesses ranging from 100 to 185 nm were used, and the results are depicted in figure 4. As illustrated, the dark electrical resistivity decreases with increasing film thickness and reaches a constant value at $1.81 \times 10^6\ \Omega$ cm. Such variation is attributed to classical size effect on the electrical resistivity of the films. Normally, when the thickness of the material becomes of the order of the mean free path, the classical size effect on the motion of charge carriers dominates.

The thickness dependence of the films in the present study is explained on the basis of Tellier's model of the size effect [34]. According to this model, the resistivity of thin films is

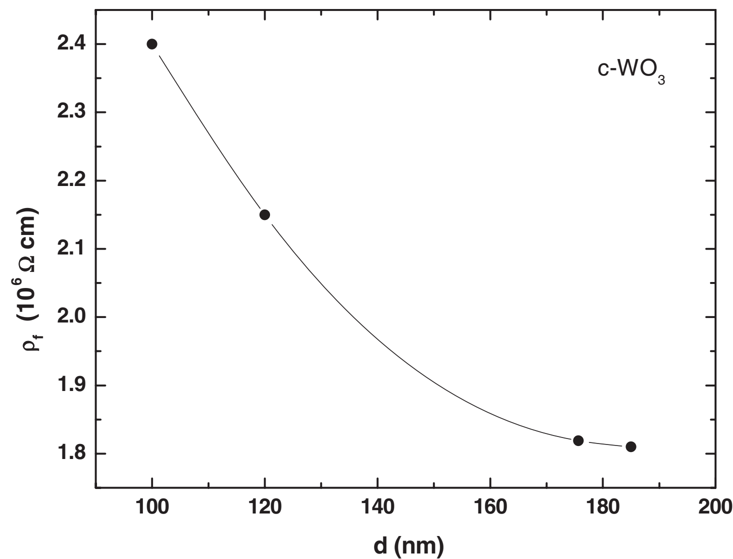

Figure 4. Dependence of the dark resistivity on film thickness for c-WO_3 films.

given by

$$\rho_f = \rho_\mathrm{b}\left[1 + \frac{3}{8}\frac{(1-p)l}{d}\right], \tag{6}$$

where ρ_b (bulk resistivity) is the resistivity of the infinitely thick material which has the same microstructure as that of films studied, p is called the specularity parameter, which varies between 0 and 1, l is the mean free path of charge carriers in the hypothetical bulk, and d is the film thickness.

The specularity parameter is an index to indicate how charge carriers are scattered at the boundary surfaces. $p = 1$ indicates that all the charge carriers are specularity scattered at the surface without any loss in the drift velocity component in the direction of the applied electric field and $p = 0$ indicates that the charge carriers are diffusely scattered with a complete loss in the direction of motion. It should be mentioned that $p = 1$ is valid for ideal single-crystalline films, but p normally approaches 0 for polycrystalline films [35]. Therefore, we assume that $p = 0$ for our polycrystalline films. With this assumption equation (1) can be written as follows:

$$\rho_\mathrm{f} d = \rho_\mathrm{b} d + \tfrac{3}{8} l \rho_\mathrm{b}. \tag{7}$$

Figure 5 shows a plot of $\rho_\mathrm{f} d$ as a function of film thickness. The linear nature of the plots indicates that the electrical resistivity exhibits size effect phenomena in these films. As is seen from the equation (7), the slopes of these plots give the bulk resistivity, ρ_b, values. The intercepts give the values of the mean free path, l, of electrons. The values of the mean free path and the bulk resistivity for c-WO_3 were found to be 289.6 nm and 1.14×10^6 Ω cm, respectively.

The temperature dependence of the DC conductivity for c-WO_3 thin films with thickness 100 nm, as a representative sample, in two environmental conditions (air and vacuum) is shown in figure 6. The conductivity, also, is higher, by one order, in films measured in air than of those measured in vacuum, which is similar to that observed in a-WO_3.

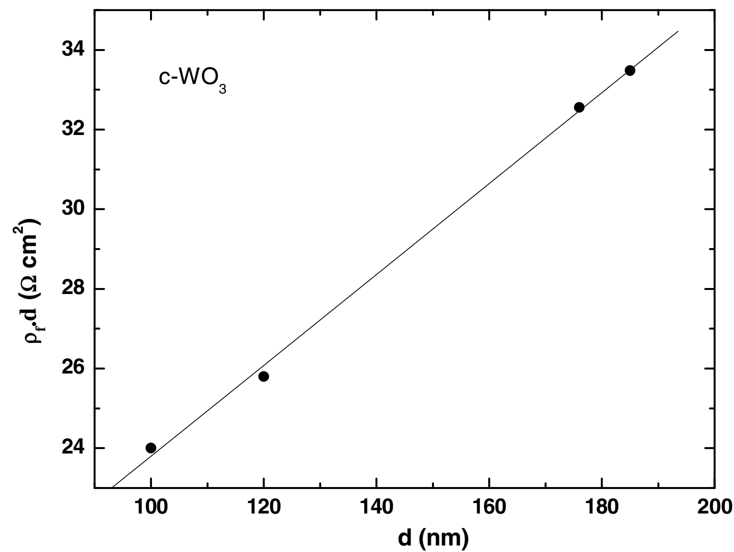

Figure 5. Variation of $\rho_f d$ with the film thickness, d, of c-WO_3 films.

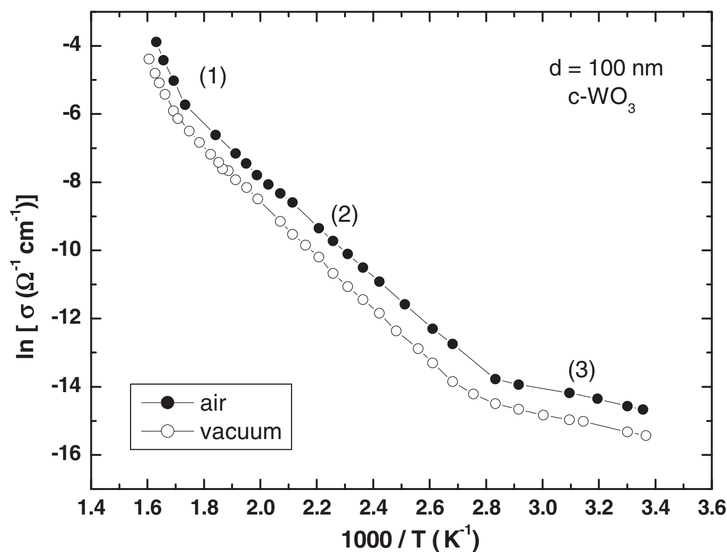

Figure 6. The relation between $\ln\sigma$ and $1000/T$ for c-WO_3 films in air and vacuum conditions.

The results indicate that the ($\ln\sigma = f(10^3/T)$) curves present three linear portions. The activation energies obtained were also found to be independent of the film thickness in the thickness range. The first one, in the higher temperature range ($T > 570$ K), is characterized by a greater slope, $\Delta E_1 = 1.54$ eV; $\Delta E_2 = 0.62$ eV for the second portion (353 K $< T <$ 570 K); and in the lower temperature range ($T < 353$ K), $\Delta E_3 = 0.15$ eV. Undoubtedly, the mechanism of electrical conduction in the samples studied can be explained by taking into account the models elaborated for films with polycrystalline (discrete) structure [36–38]. Therefore, the conduction mechanism is dominated by the inherent

intercrystallite boundaries [39–42]. Generally, the study of electronic transport properties in polycrystalline thin films is based upon the consideration that crystallite boundaries have a space charge region due to interface processes. Consequently, band bending occurs, resulting in a potential barrier to the electronic transport. This fact determines a reduction of carrier mobility and electrical conductivity of a certain material in thin films as compared to single crystals of the respective material [42]. We consider that the Seto model [43, 44] with several modifications proposed by Baccarani *et al* [46, 47] could explain the mechanism of electron transfer in the investigated films. The following assumptions were made in this model [39, 40]:

(a) The crystallites have similar size and shape, l.
(b) There is only one type of monovalent impurity at the crystallite boundary 'trapping states', uniformly distributed with a concentration N_D; the crystallite boundary contains N_t traps located at energy E_t with respect to the Fermi level (in intrinsic material) at the interface.
(c) The traps are initially neutral and become charged by trapping a free carrier.
(d) The crystallites have similar size and shape and we neglect the mobile carrier in intercrystalline boundaries (boundary width).

According to this model, for a given set of l, N_t and E_t, there is an impurity concentration, N_D^*, which indicates the degree of depletion in the film crystallites. Two conditions for impurity concentrations are possible.

- For $N_D > N_D^*$, the crystallites are partially depleted and the temperature dependence of the electrical conductivity can be determined corresponding to two energy domains [43–46].
  - (i) If $E_F - E_t - E_b \gg k_B T$, the electrical conductivity is given by [45, 46]:

$$\sigma = \frac{e^2 l N_C^2 \nu n_o}{k_B T} \exp\left(-\frac{\Delta E_1}{k_B T}\right), \tag{8}$$

where

$$\nu = \left(\frac{k_B T}{2\pi m^*}\right)^{1/2}$$

and the activation energy, ΔE_1, is equal the energy barrier at crystallite boundary, E_b, given by [45]

$$\Delta E_1 = E_b = \frac{e^2 l^2 N_D}{8\varepsilon_r}, \tag{9}$$

  - (ii) For the energy domain $E_t + E_b - E_F \gg k_B T$, the electrical conductivity of the films can be written as

$$\sigma = \frac{e N_C^2 \nu}{k_B T N_t} \left(\frac{2\varepsilon_r E_b}{N_D}\right)^{1/2} \exp\left(-\frac{\Delta E_2}{k_B T}\right), \tag{10}$$

where

$$\Delta E_2 = \tfrac{1}{2} E_g - E_t.$$

- For $N_D < N_D^*$, the electrical conductivity can be written as

$$\sigma = \frac{e^2 l^2 N_C N_D \nu}{2k_B T (N_t - l N_D)} \exp\left(-\frac{\Delta E_3}{k_B T}\right). \tag{11}$$

In equations (8)–(11), the following notation has been used: e is the electron charge, E_F is the energy of the Fermi level, N_C is the effective state density for the conduction band, n_0 is the electron concentration in the neutral domain of crystallites, m^* is the scalar effective mass of the charge carrier, ε_r is the low-frequency permittivity of the crystallites, l is the average size of the crystallites, E_g is the energy of the forbidden band, and E_t is the energy of trapping states with respect to the Fermi level at interface.

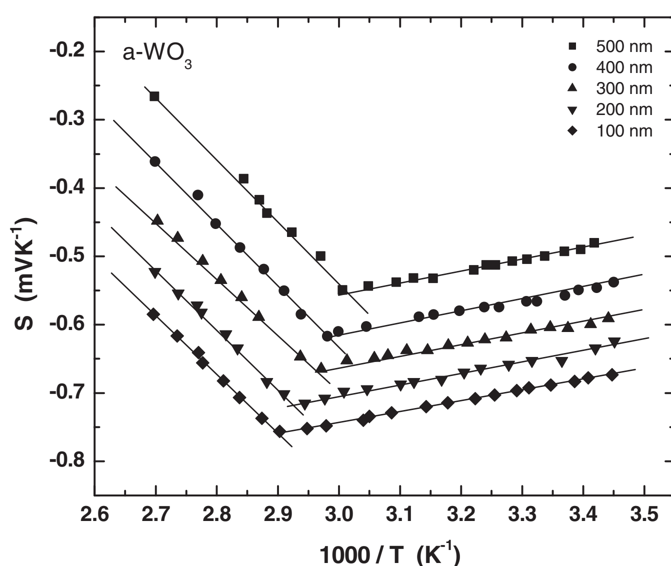

Figure 7. The variation of the Seebeck coefficient, S, against $1000/T$ for a-WO_3 films.

By assuming that in the lower temperature range ($T < 353$ K), the expression of σ in equation (8) is valid. From the slope of the $\ln \sigma = f(10^3/T)$ curve in this temperature range, the value of the energy barrier, E_b, has been calculated, and it was found to be 0.15 eV. From the slope of the second portion ($353 < T < 570$ K), the value of the trap energy E_t has been determined from equation (10) taking the value of $E_g = 3.05$ eV [15], which was found to be 0.90 eV. The value of the impurity concentration, N_D, was determined from equation (10), taking the value $\varepsilon_r = 5.12$ [15], and was found to be 4.05×10^{15} cm^{-3} eV^{-1}.

3.2. *Thermoelectric power measurements*

Figure 7 shows the temperature dependence of the thermoelectric power, S, for a-WO_3 film of thickness range 100–500 nm in the temperature range 290–370 K. The sign of S was found to be negative throughout the whole of the temperature range, indicating that the investigated samples are n-type semiconductors, as usual in metal oxide semiconductors. The same type of conduction has been observed in sputtered [9] and spray pyrolysis WO_3 films [23]. It is also clear that the magnitude of S decreases on increasing the film thickness. The linear curves obtained show that the absolute value of S gradually increases with increasing temperature and reaches a maximum at around 350 K.

At temperatures higher than 350 K, the values gradually decrease with increasing temperature. From the slope of these linear parts, the activation energy of thermoelectric power, ΔE_s, of each film thickness was calculated. It was found that the slopes of these linear parts are independent of the film thickness. The mean value of the activation energy of thermoelectric power in the first region, $T < 350$ K, is $\Delta E_{s1} = 0.16$ eV, and in the second region, $T > 350$ K, $\Delta E_{s2} = 0.85$ eV. The present experimental results for S can be understood in the light of the results of DC conductivity discussed above. In the first region, the thermoelectric power may be explained by assuming that the conduction take place by variable-range hopping (VRH). In

such a case, S has been determined as [29, 47]

$$\frac{S}{T} = -\frac{\pi^2 k^2 \gamma}{3e(n+1)} \frac{A}{T^{1/(n+1)}}, \tag{12}$$

where

$$\gamma = \frac{1}{N(E_F)} \left[\frac{dN(E)}{dE} \right]_{E=E_F}, \qquad \text{and} \qquad A = 2.1 \left(\frac{\alpha^3}{kN(E_F)} \right)^{1/4} = T_o^{1/4}$$

where $N(E_F)$ is the density of states at the Fermi level, T_o is the degree of disorder, α is the decay constant of the wavefunction of localized states at E_F, γ is the Debye frequency, and n is a dimension constant.

In the second region, $T > 350$ K, the Seebeck coefficient within the small-polaron model can be expressed by the relation [47, 48]

$$S = -\frac{k_B}{e} \left[\frac{E_s}{k_B T} + C \right], \tag{13}$$

where E_s is the activation energy for thermoelectric power and C the heat of transport.

4. Conclusions

The temperature dependence of dark electrical conductivity of a-WO_3 and c-WO_3 in two environmental conditions (air and vacuum) show three distinct regions. The mechanisms of electrical conduction in a-WO_3 are explained in terms of a simple Arrhenius law, a polaron model and a variable-range hopping model. For c-WO_3 films, the mechanism of electrical conduction is interpreted on the basis of the Seto model proposed for polycrystalline semiconducting films. It was found that the variation of resistivity with the film thickness follows the Tellier model of size effect with parameters $\rho_b = 1.14 \times 10^6$ Ω cm and $l =$ 289.6 nm. Thermoelectric power measurement shows that the films are n-type semiconductors.

References

[1] Fröbel P and Bärner K 1986 *J. Non-Cryst. Solids* **88** 329
[2] Bansal N P 1990 *J. Appl. Phys.* **68** 1143
[3] Braunstein R 1978 *Solid State Commun.* **28** 839
[4] Dautrmont-Smith W C 1982 *Displays* **3** 67
[5] Goldner R B, Chapman R L, Foley G, Goldner E L, Haas T, Norton P, Seward G and Wong K K 1986 *Sol. Energy Mater.* **14** 195
[6] Shaltout I I, Tang Y I, Braunstein R and Shaisha E E 1996 *J. Phys. Chem. Solids* **57** 1223
[7] Georg A, Graf W and Wittwer J 1998 *Sol. Energy Mater. Sol. Cells* **51** 353
[8] Wang X G, Jiang Y S, Yang N H, Yuan L and Pang S J 1999 *Appl. Surf. Sci.* **143** 135
[9] Akl A A, Kamal H and Abdel-Hady K 2003 *Physica* B **325** 65
[10] Kamal H, Akl A A and Abdel-Hady K 2004 *Physica* B **349** 192
[11] Rougier A, Portemer F, Quédé A and El-Marssi M 1999 *Appl. Surf. Sci.* **153** 1
[12] Regragui M, Addou M, Outzourhit A, Bernéde J C, El-Idrissi B, Benseddik E and Kachovane A 2000 *Thin Solid Films* **358** 40
[13] Agrawal A, Cronin J P and Zhung R 1993 *Sol. Energy Mater.* **31** 9
[14] Antonaia A, Polichetti T, Addonizio M L, Aprea S, Minarini C and Rubino A 1999 *Thin Solid Films* **354** 73
[15] Hutchins M G, Aboualkhair O, El-Nahass M M and Abd-El-Hady K 2005 *Mater. Chem. Phys.* **98** 401
[16] Krings L H M and Talen W 1998 *Sol. Energy Mater Sol. Cells* **54** 27
[17] Lee K D 1999 *Sol. Energy Mater. Sol. Cells* **57** 21
[18] Su L, Zhang L, Fang J, Xu M and Lu Z 1999 *Sol. Energy Mater. Sol. Cells* **58** 133
[19] Wang J, Bell J M and Skryabin I L 1999 *Sol. Energy Mater. Sol. Cells* **56** 465
[20] Hutichins M G, Kamel N A and Abdel-Hady K 1998 *Vacuum* **51** 433

[21] Hutchins M G, Kamel N A, El-Kadry N, Ramadan A A and Abdel-Hady K 1998 *Japan. J. Appl. Phys.* **37** 4812

[22] Özkan E and Tepehan F Z 2001 *Sol. Energy Mater. Sol. Cells* **68** 265

[23] Regragui M, Jousseaume V, Addou M, Outzourhit A, Bernéde J C and El-Idrissi B 2001 *Thin Solid Films* **397** 238

[24] Regragui M, Addou M, Outzourhit A, El-Idrissi Elb, Kachouane A and Bougrine A 2003 *Sol. Energy Mater. Sol. Cells* **77** 341

[25] Hutchins M G, Ageorges P, Butt N S and Topping J 1998 *Renew. Energy* **15** 165

[26] Stoneham A M 1987 *Solid State Gas Sensors* ed P Moseley and B Tofield (Bristol: Hilger)

[27] Ambily S and Menon C S 1999 *Thin Solid Films* **347** 284

[28] Kusters R M, Singleton J and Keen D A 1989 *Physica* B **155** 362

[29] Mott N F 1968 *J. Non-Cryst. Solids* **1** 1

[30] Mott N F and Davis E A 1979 *Electronic Processes in Non-Crystalline Materials* 2nd edn (Oxford: Clarendon)

[31] Murawski L, Chung C H and Mackenzie J D 1979 *J. Non-Cryst. Solids* **32** 91

[32] Sayer M and Mansingh A 1987 *Non-Crystalline Semiconductors* vol 3, ed M Pollak (Boca Raton, FL: CRC Press) p 1

[33] Greaves G N 1973 *J. Non-Cryst. Solids* **11** 427

[34] Tellier C R 1978 *Thin Solid Films* **51** 311

[35] Das V D and Selvaraj S 1999 *Solid State Commun.* **111** 43

[36] Volger J 1950 *Phys. Rev.* **9** 1023

[37] Petritz R L 1956 *Phys. Rev.* **104** 1508

[38] Mayadas A F and Shatzkes M 1970 *Phys. Rev.* B **1** 701

[39] Harbeke G 1985 *Polycrystalline Semiconductors: Physical Properties and Application* (Berlin: Springer)

[40] Kazmerski L L 1980 *Polycrystalline and Amorphous Thin Films and Devices* (New York: Academic) p 96

[41] Rusu G I, Popa M E, Rusu G G and Salaoru I 2003 *Appl. Surf. Sci.* **218** 222

[42] Tigau N, Rusu G I, Ciupina V, Prodan G and Vasile E 2005 *J. Optoelectron. Adv. Mater.* **7** 727

[43] Seto J Y W 1975 *J. Electrochem. Soc.* **122** 701

[44] Seto J Y W 1975 *J. Appl. Phys.* **465** 247

[45] Baccarani G, Rico B and Spandini G 1978 *J. Appl. Phys.* **49** 5565

[46] Seager C H and Gastner T G 1978 *J. Appl. Phys.* **49** 3879

[47] Singh B, Bhatia K L, Kishore N, Singh M, Malik S K and Kanjilal D 1995 *J. Non-Cryst. Solids* **91** 146

[48] Emin D 1976 *Physics of Structurally Disorder Solids* ed S S Mitra (New York: Plenum)